



Published in final edited form as:

Ultrasound Med Biol. 2016 February ; 42(2): 518–527. doi:10.1016/j.ultrasmedbio.2015.08.014.

Trans-Stent B-Mode Ultrasound and Passive Cavitation Imaging

Kevin J. Haworth^{*,†}, Jason L. Raymond[†], Kirthi Radhakrishnan^{*}, Melanie R. Moody[‡], Shao-Ling Huang[‡], Tao Peng[‡], Himanshu Shekhar^{*}, Melvin E. Klegerman[‡], Hyunggun Kim[‡], David D. Mcpherson[‡], and Christy K. Holland^{*,†}

^{*}Division of Cardiovascular Health and Disease, Department of Internal Medicine, University of Cincinnati, Cincinnati, Ohio, USA

[†]Biomedical Engineering Program, University of Cincinnati, Cincinnati, Ohio, USA

[‡]Division of Cardiology, Department of Internal Medicine, University of Texas Health Science Center at Houston, Houston, Texas, USA

Abstract

Angioplasty and stenting of a stenosed artery enable acute restoration of blood flow. However, restenosis or a lack of re-endothelialization can subsequently occur depending on the stent type. Cavitation-mediated drug delivery is a potential therapy for these conditions, but requires that particular types of cavitation be induced by ultrasound insonation. Because of the heterogeneity of tissue and stochastic nature of cavitation, feedback mechanisms are needed to determine whether the sustained bubble activity is induced. The objective of this study was to determine the feasibility of passive cavitation imaging through a metal stent in a flow phantom and an animal model. In this study, an endovascular stent was deployed in a flow phantom and in porcine femoral arteries. Fluorophore-labeled echogenic liposomes, a theragnostic ultrasound contrast agent, were injected proximal to the stent. Cavitation images were obtained by passively recording and beamforming the acoustic emissions from echogenic liposomes insonified with a low-frequency (500 kHz) transducer. *In vitro* experiments revealed that the signal-to-noise ratio for detecting stable cavitation activity through the stent was greater than 8 dB. The stent did not significantly reduce the signal-to-noise ratio. Trans-stent cavitation activity was also detected *in vivo* via passive cavitation imaging when echogenic liposomes were insonified by the 500-kHz transducer. When stable cavitation was detected, delivery of the fluorophore into the arterial wall was observed. Increased echogenicity within the stent was also observed when echogenic liposomes were administered. Thus, both B-mode ultrasound imaging and cavitation imaging are feasible in the presence of an endovascular stent *in vivo*. Demonstration of this capability supports future studies to monitor restenosis with contrast-enhanced ultrasound and pursue image-guided ultrasound-mediated drug delivery to inhibit restenosis.

Keywords

Passive acoustic mapping; Cavitation imaging; Image-guided therapy; Ultrasound contrast agent; Endovascular stent; Drug delivery; Targeted liposomes

Introduction

Drug-eluting and bare-metal stents are available for atheroma intervention after balloon angioplasty, with stent choice being dictated by patient comorbidity factors. Neo-intimal hyperplasia and vascular smooth muscle cell proliferation are important mechanisms for arterial stenosis in endogenous atheroma and restenosis within the stent post-implantation. Drug-eluting stents aim to reduce restenosis, but typically delay re-endothelization, thus necessitating long-term anti-platelet therapy (Cutlip et al. 2001; Luscher et al. 2007). Bare metal stents permit re-endothelization and reduce the risk of thrombosis, but are subject to restenosis.

Approaches to deliver therapeutics to the vascular wall may allow re-endothelization after stent deployment while inhibiting restenosis. For example, PPAR γ (peroxisome proliferator-activated receptor γ) agonists, such as rosiglitazone, have local anti-inflammatory effects in the arterial wall (Beckman et al. 2003). Like many potential therapeutics, secondary effects of systemic PPAR γ agonists have limited their clinical utility (Nissen and Wolski 2007; Zinn et al. 2008). Thus, a spatially and temporally targeted therapeutic delivery approach is attractive. An intrinsically echogenic liposome formulation has been developed that can be loaded with therapeutics (Britton et al. 2010; Buchanan et al. 2010; Huang et al. 2009; Shaw et al. 2009; Tiukinhoy et al. 2004) and serve as an ultrasound contrast agent. Echogenic liposomes (ELIP) have been loaded with both rosiglitazone and the endothelial nitric oxide synthase gene and have been reported to have an effect in stabilizing atheroma after balloon angioplasty (Huang et al. 2007, 2009). When exposed to ultrasound, the microbubbles within ELIP oscillate volumetrically. The oscillation (also referred to as cavitation [Leighton 1997]) can induce beneficial bio-effects. The ability to deliver therapeutics to the vascular wall can be enhanced when the ELIP oscillate in a particular low-amplitude mode known as stable cavitation (Hitchcock et al. 2010).

For therapeutic delivery at the site of stent placement, a number of conditions are required. To achieve stable cavitation, particular *in situ* ultrasound pressures are required (Bader and Holland 2013; Radhakrishnan et al. 2013). Heterogeneity of the overlying tissue makes it difficult to ensure *a priori* that the proper ultrasound pressure amplitude is achieved at the desired location. Techniques that rely on the passive detection of cavitation emissions from the microbubbles can be used as a feedback mechanism. Passive cavitation detection techniques implement a receive-only transducer to measure the cavitation emissions (Atchley et al. 1988). The cavitation activity may be induced by a separate therapy transducer. Passive cavitation detection techniques have been used to inform the therapeutic ultrasound insonation scheme for ultrasound-enhanced thrombolysis (Hitchcock et al. 2011). To optimize the cavitation activity throughout a targeted vessel, the cavitation activity needs to be mapped throughout the vessel. Passive cavitation imaging uses an array-based ultrasound system in receive-only mode to measure and beamform the cavitation emissions. The resulting image is a map of the cavitation activity (Gyöngy and Coussios 2010; Haworth et al. 2012; Salgaonkar et al. 2009), which can be overlaid on a standard B-mode image to create duplex passive cavitation images. The B-mode image provides anatomic information, and the overlaid cavitation activity can provide therapeutic guidance. However,

previous studies have not determined if this technique is robust enough to provide feedback through an endovascular stent.

This study had three aims. The first aim was to determine whether ultrasound can penetrate through a stent to induce stable cavitation emissions from ELIP that perfuse the lumen of the stent. The second aim was to determine whether stable cavitation emissions can be detected through a stent in a porcine model. The third aim was to determine the feasibility of beamforming the cavitation emissions to form a B-mode and cavitation duplex image. If all aims are achieved, then image-guided therapeutic delivery within the stent lumen is feasible. This technique would help guide the treatment of flow-limiting atheroma.

Methods

To achieve the aims of this study, the methods described in this section were executed. This section provides a description of the preparation for the two different echogenic liposome formulations. Both preparations encapsulated octafluoropropane (OFP), a perfluorocarbon gas. Non-targeted OFP-ELIP were used to study the feasibility of the trans-stent imaging techniques. Targeted OFP-ELIP (anti-vascular cell adhesion protein 1 [VCAM-1] rhodamine-labeled OFP-ELIP) were used to study the feasibility of image-guided drug delivery. Next, the systems and techniques used to characterize, image and cavitate the ELIP are described. These measurements were performed *in vitro* and *in vivo*, with both models described. The Methods section concludes with a description of the histologic techniques used to study the feasibility of image-guided drug delivery.

Echogenic liposome preparation

Non-targeted OFP-ELIP were made from L- α -phosphatidylcholine (chicken egg, EPC), 1,2-dipalmitoyl-*sn*-glycero-3-phosphocholine (DPPC), 1,2-dipalmitoyl-*sn*-glycero-3-[phospho-*rac*-1-glycerol] (DPPG), 1,2-dipalmitoyl-*sn*-glycero-3-phosphoethanolamine-*N*-[methoxy(polyethylene glycol)-2000] (DPPE-PEG2000) and cholesterol (CH) (Avanti Polar Lipids, Alabaster, AL, USA) (28:43:8:6:15, molar ratio). The lipids (5 mg/vial) were mixed in chloroform in a small glass vial (2-mL screw thread with PTFE/silicone septum). The chloroform was removed by evaporation under argon in a 50°C water bath with constant spinning of the vial until a thin film of lipids formed on the vial wall. The lipid film was placed under high vacuum (<13 Pa) for 4 h for complete removal of the chloroform. The lipid film was hydrated with 0.5 mL de-ionized water, heated briefly to at least 56°C and sonicated in a water bath for 5 min. A 0.5-mL volume of 0.32 M mannitol was added to the sonicated lipid sample. The samples were subjected to two freeze/thaw cycles. After the second freeze/thaw cycle, the samples were again frozen and lyophilized for 48 h. OFP gas (Specialty Gases of America, Toledo, OH, USA) was loaded into the lipid dry cake by releasing the pressure in an atmosphere of OFP. The lyophilized dry cake was stored at 4°C.

Octafluoropropane ELIP targeted to VCAM-1 were made as described above except that the lipids used were DPPC, 1,2-dioleoyl-*sn*-glycero-3-phosphocholine (DOPC), DPPG, (*N*-maleimidomethyl-cyclohexane-1-carboxy)-DPPE, rhodamine-labeled DPPE and cholesterol (Avanti Polar Lipids) in a molar ratio of 46:23:8:8:0.2:14.8. The maleimido group conjugated to the DPPE acted as a flexible linking molecule by which thiolated anti-

VCAM-1 could be conjugated to the rhodamine-labeled OFP-ELIP. Anti-VCAM-1 was thiolated by reacting 0.4 mg of monoclonal anti-human porcine VCAM-1 (clone 1G11.B1, Neomarkers, Fremont, CA, USA) and 1.6 mg of non-specific mouse immunoglobulin G (Rockland Immunochem, Gilbertsville, PA, USA) with 3-(2-pyridyldithiolpropionic acid)-*N*-hydroxysuccinimide ester (SPDP) at a molar ratio of 15:1 for 30 min at $24 \pm 1^\circ\text{C}$. Protein was separated from unreacted SPDP by gel chromatography on a 50-mL Sephadex G-50 column (Sigma-Aldrich, St. Louis, MO, USA) equilibrated with 0.05 M citrate-phosphate buffer at a pH of 5.5. Protein fractions were identified using a spectrophotometric technique (Genesys 10 UV, Thermo Electron, Milford, MA, USA) at a wavelength of 280 nm, pooled and concentrated to 2 mL using Centricon YM-10 centrifugal filter units (Millipore, Billerica, MA, USA). The SPDP-activated protein was reduced in 25 mM dithiothreitol for 30 min at $24 \pm 1^\circ\text{C}$. Thiolated anti-VCAM-1 was isolated using a Sephadex G-50 column, equilibrated, and eluted with pH 6.7 citrate-phosphate buffer. The thiolated anti-VCAM-1 was incubated with reconstituted ELIP (10 mg lipid/mL, 0.1 M phosphate buffer at a pH of 6.62) under argon overnight at $24 \pm 1^\circ\text{C}$ to produce anti-VCAM-1 rhodamine-labeled ELIP. The anti-VCAM-1 rhodamine-labeled ELIP were separated from free protein and low-molecular-weight products by gel filtration on a 20-mL Sepharose CL-4B column (Sigma-Aldrich) that had been pre-saturated with unconjugated, unlabeled ELIP according to the method of Lasch et al. (2003) and eluted with 0.02 M phosphate-buffered saline (containing 90 mM sodium chloride to render the liposomes isotonic when reconstituted) at a pH of 7.4. The anti-VCAM-1 rhodamine-labeled OFP-ELIP were lyophilized with 0.1 M D-mannitol. A quantitative immunoblot assay for liposomal immunoglobulin G (Klegerman et al. 2002) was used to determine that the anti-VCAM-1 was conjugated to the OFP-ELIP with an efficiency of $3.8 \mu\text{g}$ antibody/ mg lipid (20% of total anti-VCAM-1 reacted) equivalent to 1,055 molecules/liposome.

Before use, both non-targeted OFP-ELIP and anti-VCAM-1 rhodamine-labeled OFP-ELIP were evacuated ($\sim 85\%$ vacuum) and subsequently re-pressurized by adding 4 mL of OFP gas (2 atm or 0.2 MPa) to the sealed vial using a syringe. The vials remained pressurized for at least 45 min before being vented to 1 atm (0.1 MPa) of pressure and reconstituted with air-saturated de-ionized water to a lipid concentration of 10 mg/mL. All OFP-ELIP were used immediately after reconstitution.

Characterization of OFP-ELIP

The stability of non-targeted OFP-ELIP was measured and compared with that of Definity (perflutren lipid microspheres; Lantheus Medical Imaging, North Billerica, MA, USA), a Food and Drug Administration-approved ultrasound contrast agent consisting of octofluoropropane gas encapsulated by a lipid shell. Vials of Definity were activated according to the manufacturer's instructions. The frequency-dependent acoustic attenuation and particle size distribution of non-targeted OFP-ELIP and Definity were determined using the methods outlined in Raymond et al. (2014). Briefly, a broadband substitution technique was used every 60 s to determine the frequency-dependent acoustic attenuation coefficient for each ultrasound contrast agent over 100 min. The ultrasound contrast agents were diluted (OFP-ELIP 1:100, Definity 1:2,000) into air-saturated phosphate-buffered saline mixed with 0.5% (w/v) bovine serum albumin solution (Sigma-Aldrich) maintained at $37 \pm 0.5^\circ\text{C}$. The

initial size distribution of the ultrasound contrast agents was measured using a Multisizer 4 with a 30- μ m aperture (Beckman Coulter, Brea, CA, USA) to determine the number density.

Ultrasound imaging procedures

In vivo B-mode ultrasound images were acquired using an HDI-5000 ultrasound scanner (Philips Healthcare, Bothell, WA, USA) with an L12-5 (38 mm) linear array probe (ATL Ultrasound, Bothell, WA, USA). *In vitro* B-mode ultrasound images were acquired using a Vantage ultrasound system (Verasonics, Kirkland, WA, USA) with a P4-1 phased array probe (ATL Ultrasound). The acoustic output of both imaging systems was set as low as possible while still producing an image with adequate contrast. The imaging parameters for the *in vivo* images were optimized manually by an experienced echocardiologist.

In vitro and *in vivo* duplex passive cavitation images were obtained with the Vantage ultrasound system using the P4-1 phased array (Fig. 1a). Each duplex image data set consisted of two successive acquisitions of 40 frames of passively acquired cavitation data and 15 frames of B-mode data (Fig. 1b). The passively acquired data were synchronous with the 500-kHz therapeutic ultrasound pulses (see below). B-Mode images were acquired at a frame rate of 10 Hz. The passively acquired data were beamformed using 40-kHz bands centered about the ultraharmonic frequencies of 2.25, 2.75 and 3.25 MHz (Haworth et al. 2012) to form passive cavitation images of stable cavitation activity (Hitchcock et al. 2010; Sutton et al. 2013). The total energy in these ultraharmonic bands was summed across each acquisition to form a single image of cumulative emissions.

Cavitation induction

A therapeutic transducer (35 mm diameter, unfocused; H152, Sonic Concepts, Bothell, WA, USA) operating at a 500-kHz center frequency was used to induce stable cavitation activity using peak rarefactional pressures of 170 kPa (mechanical index = 0.24) and 360 kPa (mechanical index = 0.51) (Fig. 1a). All acoustic pressures were measured at 37°C in a water tank and were not de-rated for attenuation. The uncertainty in the measurements was $\pm 15\%$. Therapeutic insonation consisted of 100-cycle pulses repeated at a pulse repetition period of 10 ms. The imaging array and the therapeutic transducer were co-registered using a rigid custom holder similar to the design used by Zhang et al. (2010) (Fig. 1a).

In vitro experiments

To ascertain the effect of the stent on cavitation activity and imaging quantitatively, *in vitro* experiments were performed with and without a stent (Express SD renal/biliary 6 \times 14 mm, Boston Scientific, Marlborough, MA, USA). The stent was deployed in a 6.3-mm-inner-diameter latex tube flow phantom immersed in a water bath filled with degassed water at 37°C. The spatial orientation of the transducers and flow phantom mimicked the *in vivo* experiments (Fig. 1a). Either degassed saline or non-targeted OFP-ELIP (0.05 mg of lipid/mL) flowed through the system. Duplex passive cavitation image data sets were obtained during therapeutic insonation (Fig. 1b). The peak rarefactional pressure amplitude was adjusted in steps of approximately 24 kPa between 65 and 360 kPa. For each vial of non-targeted OFP-ELIP, two duplex passive cavitation image data sets were acquired at each pressure amplitude, and passive cavitation images formed. Measurements were

repeated for six vials of non-targeted OFP-ELIP. The measured power spectra used to compute the passive cavitation images were averaged over a region of interest defined by the spatial extent of the stent. The same spatial coordinates were used to define the region of interest with and without the stent. Ultraharmonic cavitation activity, defined as the sum of the power in 40-kHz-wide bands centered at 2.25, 2.75 and 3.25 MHz, and inharmonic cavitation activity, defined as the sum of the power in 31-kHz-wide bands centered at 2.305, 2.805 and 3.305 MHz, were computed. The width of the ultraharmonic bands was selected based on the bandwidth of the transmitted pulse. Location and width of the inharmonic bands were empirically determined to minimize the inclusion of spectral leakage from harmonic and ultraharmonic emissions. The signal-to-noise ratio (SNR) for each insonation pressure amplitude was computed as the ratio of ultraharmonic power to inharmonic power.

***In vivo* experiments**

All animal studies were approved by the Animal Welfare Committee at the University of Texas Health Science Center at Houston. Two Yucatan miniswine (28 and 33 kg) were anesthetized with ketamine (35 mg/kg) and xylazine (5 mg/kg) and maintained on isoflurane gas (1%–3%). The carotid artery was exposed and used for vascular access. Under fluoroscopic guidance, each common femoral artery was denuded using a 4F Fogarty catheter (Gal et al. 1990; White et al. 1988).

A stent (Express SD renal/biliary 6 × 18 mm, Boston Scientific) was deployed in each common femoral artery under fluoroscopic guidance, and a 6F catheter was placed immediately proximal to the stent. OFP-ELIP were injected into the femoral artery through the catheter. The therapeutic transducer was aimed at the stent under B-mode and color Doppler guidance using the co-registered P4-1 array.

After targeting, a single duplex passive cavitation image data set was acquired as a control before injecting non-targeted OFP-ELIP. Thereafter, a 2.5-mL bolus of non-targeted OFP-ELIP (5 mg of lipid) was infused gently over approximately 30 s. Duplex image data sets were acquired approximately every 12 s during the bolus injection. Five infusions of non-targeted OFP-ELIP were performed for each stent, with approximately 1 min between injections.

To assess the feasibility of drug delivery to the vascular wall beyond the stent, a final 2.5-mL bolus injection of anti-VCAM-1 rhodamine-labeled OFP-ELIP (5 mg of lipid) was injected into the lumen of the artery and exposed to the therapeutic ultrasound. The ultrasound parameters and timing were identical to those for earlier experiments (Fig. 1b). One artery was not exposed to ultrasound to serve as a negative control.

Histology

After euthanasia, the femoral arteries were harvested and cut longitudinally through both tissue and stent, and the stent carefully removed. The arteries were cut into 2- to 3-mm segments, placed in optimal cutting temperature compound and frozen on dry ice. Segments were cut into 5- μ m sections and examined using a Nikon Optiphot brightfield/darkfield inverted microscope at 60 \times magnification (Nikon Instruments, Melville, NY, USA).

Fluorescence images were taken with a fluorescein isothiocyanate (FITC) filter and a tetramethylrhodamine (TRITC) filter. Autofluorescence of the tissue was observed with the FITC filter and used to identify the lumen and media of the vascular wall. Delivery into the vascular wall of the rhodamine-labeled lipids within the anti-VCAM-1 rhodamine-labeled OFP-ELIP was observed using the TRITC filter.

Results

Characterization of non-targeted OFP-ELIP

The number density used for attenuation measurements of non-targeted OFP-ELIP (1:100 dilution) was $(135 \pm 49) \times 10^6$ ELIP/mL, and that for Definity (1:2,000 dilution) was $(5.2 \pm 0.8) \times 10^6$ microbubbles/mL. In-vial number densities were 1.35×10^{10} micro-bubbles/mL for non-targeted OFP-ELIP and 1.04×10^{10} microbubbles/mL for Definity. The number-weighted size distributions of Definity (Raymond et al. 2014) and OFP-ELIP were comparable. Mean attenuation at low diagnostic ultrasound frequencies (2–10 MHz) for Definity was 23.8 dB/cm initially and 14.0 dB/cm after 100 min (Fig. 2a). For non-targeted OFP-ELIP, mean attenuation (2–10 MHz) was 14.2 dB/cm initially and 5.8 dB/cm after 100 min (Fig. 2b). At high diagnostic ultrasound frequencies (10–25 MHz), mean attenuation for Definity was 14.9 dB/cm initially and 6.8 dB/cm after 100 min (Fig. 2a). For non-targeted OFP-ELIP, mean attenuation (10–25 MHz) was 16.9 dB/cm initially and 10.8 dB/cm after 100 min (Fig. 2b). These data indicate that non-targeted OFP-ELIP have dissolution characteristics similar to those of Definity.

Trans-stent B-mode imaging of non-targeted OFP-ELIP

B-Mode images revealed that both the proximal and distal walls of the stent (relative to the imaging array) were echogenic *in vivo* at 6 MHz using the L12-5 linear array (Fig. 3a) and *in vitro* at 2.5 MHz using the P4-1 phased array (Fig. 3c). Shadowing beyond the proximal wall was minimal. Injection of non-targeted OFP-ELIP into the lumen of the vessel and latex tube resulted in a visible increase in echogenicity within the lumen of the stent (Fig. 3b, d). The large elevational beamwidth introduced acoustic clutter within the stent lumen from out-of-plane stent struts (Fig. 3c).

Effect of the stent on *in vitro* detected cavitation activity

Consistent stable cavitation activity was detected in the *in vitro* flow phantom at peak rarefactional pressures >100 kPa. Within the region of interest defined by the lumen of the stent, the SNR (defined as the ratio of spatially averaged ultraharmonic to inharmonic cavitation power within the stent [Fig. 3c]) was observed to decrease with increasing insonation pressure. The mean absolute difference in SNR as calculated with and without the stent across all pressure amplitudes was 0.5 ± 0.9 dB (Fig. 4).

Feasibility of *in vivo* cavitation imaging

Stable cavitation activity was mapped within a user-defined region, which is outlined by a *cyan box* in the representative images in Figure 5. All passive cavitation images used the same imaging algorithm and color map to allow direct comparison. In the absence of non-targeted OFP-ELIP, stable cavitation was not observed at rarefactional pressures of 170 and

360 kPa (Fig. 5a, b). When non-targeted OFP-ELIP were present in the lumen of the stent, stable cavitation activity was observed (Fig. 5c, d). In general, the 360-kPa insonation resulted in a higher peak amplitude of cavitation energy. The energy was also spread over a larger spatial area compared with that for the 170-kPa insonation. In one vessel exposed to both non-targeted OFP-ELIP and therapeutic ultrasound, no ultraharmonic emissions were detected.

Feasibility of *in vivo* drug delivery

Composite fluorescence images did not show an increase in red fluorescence in the arterial wall of the control artery where therapeutic ultrasound was not applied (Fig. 6a). The other three arteries were insonified with the therapeutic ultrasound and infused with anti-VCAM-1 rhodamine-labeled OFP-ELIP. Two arteries had detectable ultraharmonic emissions. In these arteries, there was excellent rhodamine-labeled liposome delivery to the artery wall (Fig. 6c, d). For the artery with no ultraharmonic emissions, there was no evidence of liposomal delivery to the artery wall (Fig. 6b).

Discussion

In-stent restenosis is a major challenge in the treatment of atherosclerosis. Although drug-eluting stents are useful in preventing in-stent restenosis, they necessitate long-term anti-platelet therapy to prevent stent thrombosis. Bare metal stents allow for re-endothelialization, but create inflammatory responses resulting in in-stent restenosis. Thus, the ability to deliver therapeutics that can reduce neo-intimal hyperplasia, inhibit smooth muscle cell proliferation and promote endothelialization of the stent may improve luminal patency after intravascular interventions. However, many of the potential therapeutics have unacceptable side effects when delivered systemically. Ultrasound-mediated drug delivery can provide temporally and spatially localized drug delivery. We have previously reported that stable cavitation of echogenic liposomes is concomitant with delivery to the arterial wall (Hitchcock et al. 2010). Ultrasound-mediated delivery of therapeutics to the vascular wall after stent deployment requires transmission of the ultrasound through the stent to induce cavitation. Furthermore, stable cavitation emissions must be detectable through the stent to provide image-guided feedback.

To pursue these aims *in vivo*, novel ELIP formulations were used that incorporated OFP gas. OFP is used in ultrasound contrast agents to promote the longevity of echogenicity (Ferrara et al. 2007; Sarkar et al. 2009). The solubility of OFP in an aqueous medium is approximately 30 times less than that in air, resulting in a modeled increase in longevity of a factor of 90 (Sarkar et al. 2009). The permeability of OFP through a lipid shell is about 20 times lower than that for air, which also contributes to a modeled increase in longevity (Sarkar et al. 2009). The size, number count and attenuation of the OFP-ELIP formulated for this study were comparable to prior measurements of ELIP (Raymond et al. 2014).

Our results indicate that contrast enhancement from non-targeted OFP-ELIP was observable within the lumen of an endovascularly deployed stent using B-mode ultrasound imaging. B-Mode imaging requires both transmission and reception of ultrasound through the stent. Stents with more closely spaced struts may provide greater attenuation. Moving to lower

center frequencies for B-mode and ultraharmonic passive cavitation imaging (2–4 MHz) may help compensate for the attenuation due to the stent and intervening tissue path. Diffraction of the beam through the stent struts will decrease at lower center frequencies. Additionally, the fraction of incident energy that is transmitted through a thin layer increases with decreasing frequency (Pierce 1989). The incorporation of contrast-specific or other non-linear imaging strategies, such as pulse inversion imaging and harmonic imaging, could also improve trans-stent imaging of ultrasound contrast agents by reducing acoustic clutter and imaging at a higher frequency.

Cavitation of both the non-targeted OFP-ELIP and the anti-VCAM-1 rhodamine-labeled OFP-ELIP could be induced and detected through the stent using a 500-kHz insonation. The SNR measured *in vitro* decreased with increasing insonation pressure, particularly for pressures >225 kPa. This decrease was likely due to inertial cavitation. The broadband emissions from sporadic inertial cavitation began to contribute to the power measured in the inharmonic bands (i.e., the noise in the SNR computation) at insonation pressures greater than approximately 200 kPa (data not shown). Inertial cavitation also likely depleted cavitation nuclei, thereby reducing the stable cavitation emissions (Goertz et al. 2010; Hitchcock et al. 2011). The SNR measured *in vitro* was approximately 11 dB when no inertial cavitation was present. This SNR was limited by spectral leakage from the neighboring harmonics. Spectral leakage can normally be reduced by windowing the measured cavitation emissions before computing the power spectrum. However, the most appropriate method for windowing is not obvious when performing passive cavitation imaging because of the time delays necessary for beamforming. Appropriate windowing will be an area of future investigation. No significant difference was observed between the SNRs computed with and without the stent, likely because the noise (which came predominately from spectral leakage from the harmonics) was also attenuated approximately the same amount as the signal (i.e., ultraharmonic emissions).

In vivo passive cavitation imaging mapped stable cavitation activity to the anticipated location, which was based on the insonation beam profile and the location of contrast-enhancement from both the stent and the OFP-ELIP. The anticipated location extended over an area of approximately 1–2 cm. Observation of individual cavitation image frames revealed that the centroid of cavitation activity moved within the anticipated location. The movement of the centroid was likely due to the stochastic nature of cavitation and illustrates the need for cavitation imaging.

The frequency range used to produce passive cavitation images was limited by the P4-1 transducer bandwidth and the default frequency filtering implemented by the Vantage scanner to minimize aliasing. This frequency range is similar to the frequency range used in prior transcranial passive cavitation imaging studies *in vivo* (Arvanitis et al. 2013). Higher-frequency (10.25 MHz) *in vivo* passive cavitation imaging was recently reported in superficial tumors in mice with a linear array with a higher center frequency (Choi et al. 2014). In general, the frequency limitations of passive cavitation imaging are expected to be similar to those of B-mode imaging.

Although we observed excellent stable cavitation in two arteries, we did not in a third artery. The failure to detect bubble activity in the third artery may have been the result of poor transducer alignment or some other mechanical factor. For the two arteries in which stable cavitation was detected, marked rhodamine delivery to the vascular wall was observed. When no bubble activity was detected, no delivery was observed. This result is consistent with our prior *ex vivo* work in murine arteries that revealed ultrasound-mediated delivery into the arterial wall using stable cavitation (Hitchcock et al. 2010). Our results indicate the value passive cavitation imaging may have in providing feedback and potentially guiding ultrasound-mediated drug delivery.

Model limitations

The number of arteries evaluated (4) was small in this feasibility study. The region of interest was fixed within the imaging field in this prototype image-guided therapeutic ultrasound system, which limited the ability of the technician to align the stent optimally within the imaging field. To study enhanced therapeutic delivery, the lipid shell of the anti-VCAM-1 OFP-ELIP was labeled with a fluorophore. Here, histology highlights where the lipid remnants were delivered, which may not have the same delivery profile of an encapsulated therapeutic, particularly if the therapeutic is dissolved within the aqueous core of ELIP. Delivery profiles were also likely affected by the use of non-calcified and non-atheromatous vessels.

Conclusions

This study revealed that both B-mode ultrasound imaging and passive cavitation imaging can be performed *in vivo* through a stent. The stent did not significantly reduce the passive cavitation imaging signal-to-noise ratio relative to no stent. Fluorescence histology supported the use of passive cavitation imaging to guide ultrasound-mediated drug delivery to the vascular wall at the site of stent deployment. This work indicates the feasibility of this novel imaging methodology for guided therapeutic delivery to stented arteries and opens the way for the development of therapeutics that will aid in the stabilization of atheroma at the time of mechanical intervention.

Acknowledgments

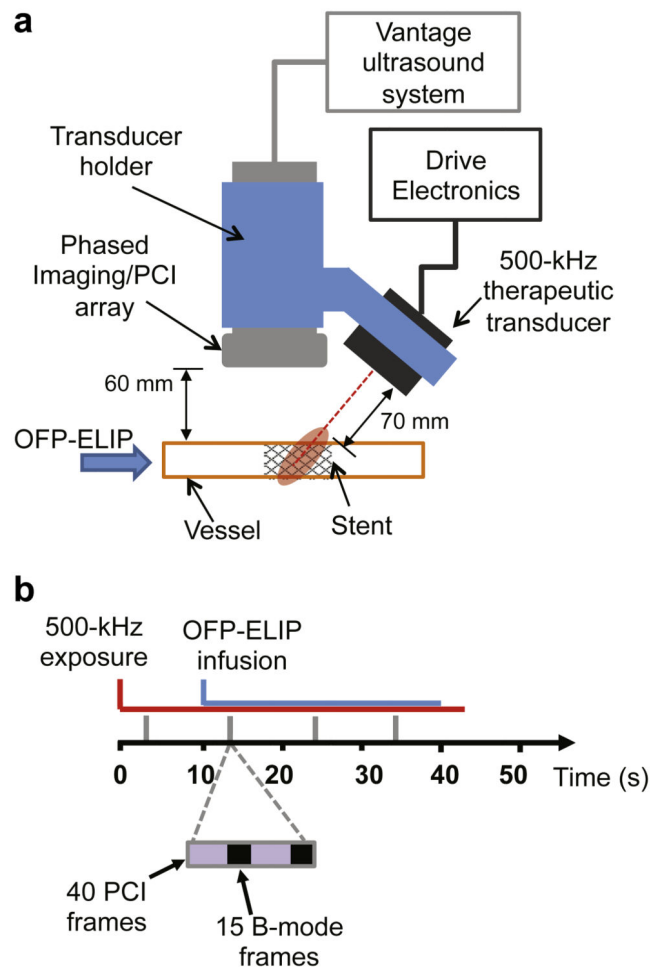
The authors also gratefully acknowledge funding support from the National Institutes of Health via grant number R01 HL074002.—The authors received assistance from James Amirian in stent procurement, Patrick H. Kee and Prakash Balan in stent deployment and Deborah Vela in histology preparation. This work was performed at the University of Cincinnati and the University of Texas Health Science Center at Houston.

References

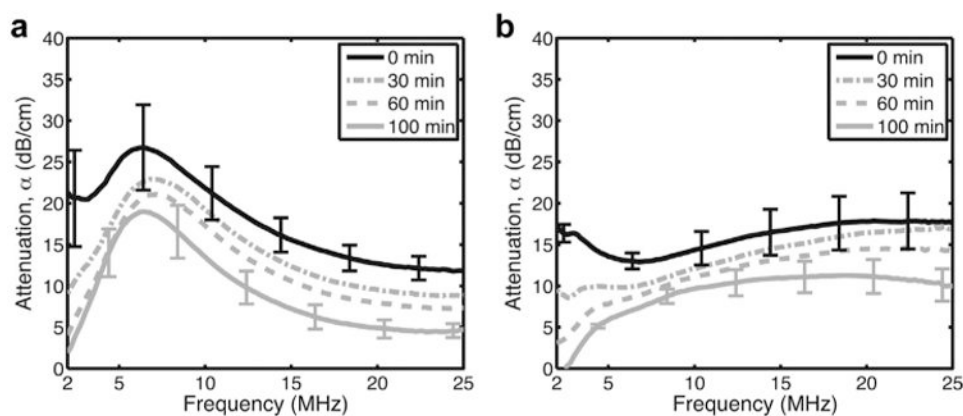
- Arvanitis CD, Livingstone MS, McDannold N. Combined ultrasound and MR imaging to guide focused ultrasound therapies in the brain. *Phys Med Biol*. 2013; 58:4749–4761. [PubMed: 23788054]
- Atchley AA, Frizzell LA, Apfel RE, Holland CK, Madanshetty SI, Roy RA. Thresholds for cavitation produced in water by pulsed ultrasound. *Ultrasonics*. 1988; 26:280–285. [PubMed: 3407017]
- Bader KB, Holland CK. Gauging the likelihood of stable cavitation from ultrasound contrast agents. *Phys Med Biol*. 2013; 58:127. [PubMed: 23221109]

- Beckman J, Raji A, Plutzky J. Peroxisome proliferator activated receptor gamma and its activation in the treatment of insulin resistance and atherosclerosis: Issues and opportunities. *Curr Opin Cardiol*. 2003; 18:479–485. [PubMed: 14597889]
- Britton GL, Kim H, Kee PH, Aronowski J, Holland CK, McPherson DD, Huang SL. In vivo therapeutic gas delivery for neuroprotection with echogenic liposomes. *Circulation*. 2010; 122:1578–1587. [PubMed: 20921443]
- Buchanan KD, Huang SL, Kim H, McPherson DD, MacDonald RC. Encapsulation of NF- κ B decoy oligonucleotides within echogenic liposomes and ultrasound-triggered release. *J Control Release*. 2010; 141:193–198. [PubMed: 19804805]
- Choi JJ, Carlisle RC, Coviello C, Seymour L, Coussios CC. Non-invasive and real-time passive acoustic mapping of ultrasound-mediated drug delivery. *Phys Med Biol*. 2014; 59:4861–4877. [PubMed: 25098262]
- Cutlip DE, Baim DS, Ho KK, Popma JJ, Lansky AJ, Cohen DJ, Carrozza JP, Chauhan MS, Rodriguez O, Kuntz RE. Stent thrombosis in the modern era: A pooled analysis of multicenter coronary stent clinical trials. *Circulation*. 2001; 103:1967–1971. [PubMed: 11306525]
- Ferrara K, Pollard R, Borden M. Ultrasound microbubble contrast agents: Fundamentals and application to gene and drug delivery. *Annu Rev Biomed Eng*. 2007; 9:415–447. [PubMed: 17651012]
- Gal D, Rongione AJ, Slovenkai GA, DeJesus ST, Lucas A, Fields CD, Isner JM. Atherosclerotic Yucatan microswine: An animal model with high-grade, fibrocalcific, nonfatty lesions suitable for testing catheter-based interventions. *Am Heart J*. 1990; 119:291–300. [PubMed: 2301218]
- Goertz DE, Wright C, Hynynen K. Contrast agent kinetics in the rabbit brain during exposure to therapeutic ultrasound. *Ultrasound Med Biol*. 2010; 36:916–924. [PubMed: 20447757]
- Gyöngy M, Coussios CC. Passive spatial mapping of inertial cavitation during HIFU exposure. *IEEE Trans Biomed Eng*. 2010; 57:48–56. [PubMed: 19628450]
- Haworth KJ, Mast TD, Radhakrishnan K, Burgess MT, Kopechek JA, Huang SL, McPherson DD, Holland CK. Passive imaging with pulsed ultrasound insonations. *J Acoust Soc Am*. 2012; 132:544–553. [PubMed: 22779500]
- Hitchcock KE, Caudell DN, Sutton JT, Klegerman ME, Vela D, Pyne-Geithman GJ, Abruzzo T, Cry PEP, Geng YJ, McPherson DD, Holland CK. Ultrasound-enhanced delivery of targeted echogenic liposomes in a novel ex vivo mouse aorta model. *J Control Release*. 2010; 144:288–295. [PubMed: 20202474]
- Hitchcock KE, Ivancevich NM, Haworth KJ, Caudell Stamper DN, Vela DC, Sutton JT, Pyne-Geithman GJ, Holland CK. Ultrasound-enhanced rt-PA thrombolysis in an ex vivo porcine carotid artery model. *Ultrasound Med Biol*. 2011; 37:1240–1251. [PubMed: 21723448]
- Huang SL, Kee P, McPherson DD, MacDonald RC. Multi-functional echogenic liposomes for image-guided and ultrasound-controlled PPAR agonist delivery. *J Am Coll Cardiol*. 2007; 49:365A.
- Huang SL, Kee PH, Kim H, Moody MR, Chrzanowski SM, MacDonald RC, McPherson DD. Nitric oxide-loaded echogenic liposomes for nitric oxide delivery and inhibition of intimal hyperplasia. *J Am Coll Cardiol*. 2009; 54:652–659. [PubMed: 19660697]
- Klegerman ME, Hamilton AJ, Huang SL, Tiukinhoy SD, Khan AA, MacDonald RC, McPherson DD. Quantitative immunoblot assay for assessment of liposomal antibody conjugation efficiency. *Anal Biochem*. 2002; 300:46–52. [PubMed: 11743691]
- Lasch, J.; Weissig, V.; Brandl, M. Preparation of liposomes. In: Torchilin, VP.; Weissig, V., editors. *Liposomes*. New York: Oxford University Press; 2003. p. 24–25.
- Leighton, TG. *The acoustic bubble*. San Diego: Academic Press; 1997.
- Lüscher TF, Steffel J, Eberli FR, Joner M, Nakazawa G, Tanner FC, Virmani R. Drug-eluting stent and coronary thrombosis: Biological mechanisms and clinical implications. *Circulation*. 2007; 115:1051–1058. [PubMed: 17325255]
- Nissen SE, Wolski K. Effect of rosiglitazone on the risk of myocardial infarction and death from cardiovascular causes. *N Engl J Med*. 2007; 356:2457–2471. [PubMed: 17517853]
- Pierce, AD. *Acoustics: An introduction to its physical principles and applications*. Woodbury, NY: Acoustical Society of America; 1989.

- Radhakrishnan K, Bader KB, Haworth KJ, Kopechek JA, Raymond JL, Huang SL, McPherson DD, Holland CK. Relationship between cavitation and loss of echogenicity from ultrasound contrast agents. *Phys Med Biol*. 2013; 58:6541–6563. [PubMed: 24002637]
- Raymond JL, Haworth KJ, Bader KB, Radhakrishnan K, Griffin JK, Huang SL, McPherson DD, Holland CK. Broadband attenuation measurements of phospholipid-shelled ultrasound contrast agents. *Ultrasound Med Biol*. 2014; 40:410–421. [PubMed: 24262056]
- Salgaonkar VA, Datta S, Holland CK, Mast TD. Passive cavitation imaging with ultrasound arrays. *J Acoust Soc Am*. 2009; 126:3071–3083. [PubMed: 20000921]
- Sarkar K, Katiyar A, Jain P. Growth and dissolution of an encapsulated contrast microbubble: Effects of encapsulation permeability. *Ultrasound Med Biol*. 2009; 35:1385–1396. [PubMed: 19616160]
- Shaw GJ, Meunier JM, Huang SL, Lindsell CJ, McPherson DD, Holland CK. Ultrasound-enhanced thrombolysis with tPA-loaded echogenic liposomes. *Thromb Res*. 2009; 124:306–310. [PubMed: 19217651]
- Sutton JT, Haworth KJ, Pyne-Geithman GJ, Holland CK. Ultrasound-mediated drug delivery for cardiovascular disease. *Expert Opin Drug Deliv*. 2013; 10:573–592. [PubMed: 23448121]
- Tiukinhoy SD, Khan AA, Huang SL, Klegerman ME, MacDonald RC, McPherson DD. Novel echogenic drug-immunoliposomes for drug delivery. *Invest Radiol*. 2004; 39:104–110. [PubMed: 14734925]
- White CJ, Ramee SR, Card HG, Abrahams LA, Svinarich JT, Wade CE, Rodkey WG, Virmani R. Laser angioplasty: An atherosclerotic swine model. *Lasers Surg Med*. 1988; 8:318–321. [PubMed: 2969072]
- Zhang M, Fabiilli ML, Haworth KJ, Fowlkes JB, Kripfgans OD, Roberts WW, Ives KA, Carson PL. Initial investigation of acoustic droplet vaporization for occlusion in canine kidney. *Ultrasound Med Biol*. 2010; 36:1691–1703. [PubMed: 20800939]
- Zinn A, Felson S, Fisher E, Schwartzbard A. Reassessing the cardiovascular risks and benefits of thiazolidinediones. *Clin Cardiol*. 2008; 31:397–403. [PubMed: 18781598]

**Fig. 1.**

Orientation of ultrasound transducers and timing diagram. (a) The P4-1 imaging array and 500-kHz therapeutic transducer were rigidly fixed in position with a prototype transducer holder. B-mode images were used to align the focal zone of the therapeutic transducer with the stent. (b) Timing diagram depicting therapeutic ultrasound exposure, OFP-ELIP infusion and data acquisition. The first duplex passive cavitation image data set (40 PCI frames, 15 B-mode frames, 40 PCI frames and, finally, 15 B-mode frames) was acquired after the start of OFP-ELIP injection. Duplex passive cavitation image data sets were acquired approximately every 12 s. OFP-ELIP infusion began around 10 s after the therapeutic ultrasound was initiated. OFP-ELIP = octafluoropropane echogenic liposomes.

**Fig. 2.**

Acoustic attenuation measurements to assess temporal stability. Frequency-dependent attenuation coefficients (error bars indicate standard errors) for (a) Definity and (b) non-targeted OFP-ELIP. The number density of contrast agent particles was $(5.2 \pm 0.8) \times 10^6/\text{mL}$ for Definity and $(135 \pm 49) \times 10^6/\text{mL}$ for OFP-ELIP. OFP-ELIP = octafluoropropane echogenic liposomes.

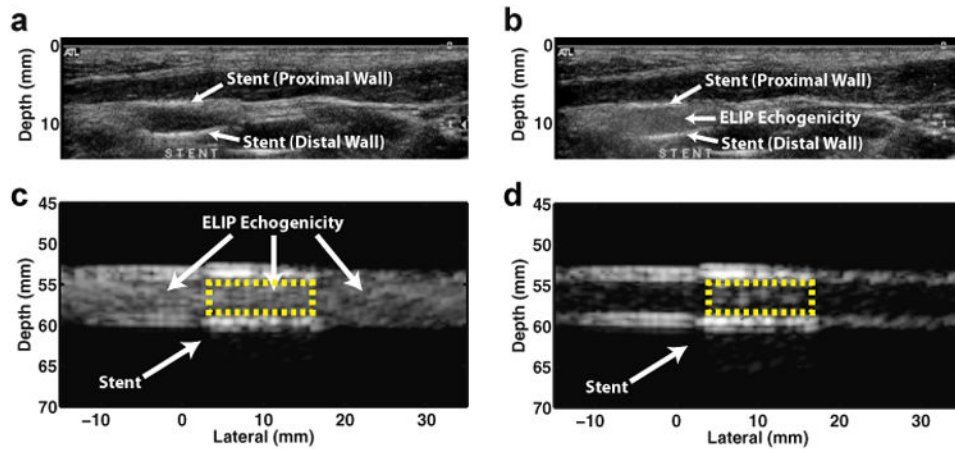


Fig. 3.

Ultrasound imaging of stent and OFP-ELIP. (a, b) B-Mode images of a stent deployed *in vivo* were acquired with the L12-5 linear array without (a) and with (b) OFP-ELIP injected into the femoral artery lumen. (c, d) B-Mode images of the stent deployed in a latex tube were acquired with a P4-1 phased array without (c) and with (d) OFP-ELIP. In all four images, the proximal and distal walls of the stent are visualized as bands of hyper-echogenicity. The wider elevational focal width of the P4-1 resulted in a noticeable artifact as the out-of-plane struts appeared in the lumen of the latex tube (c). The echogenicity of OFP-ELIP is easily observed both *in vitro* and *in vivo* (b and d). The yellow dotted boxes (c and d) denote the regions of interest used to calculate the signal-to-noise ratios plotted in Figure 4. OFP-ELIP = octafluoropropane echogenic liposomes.

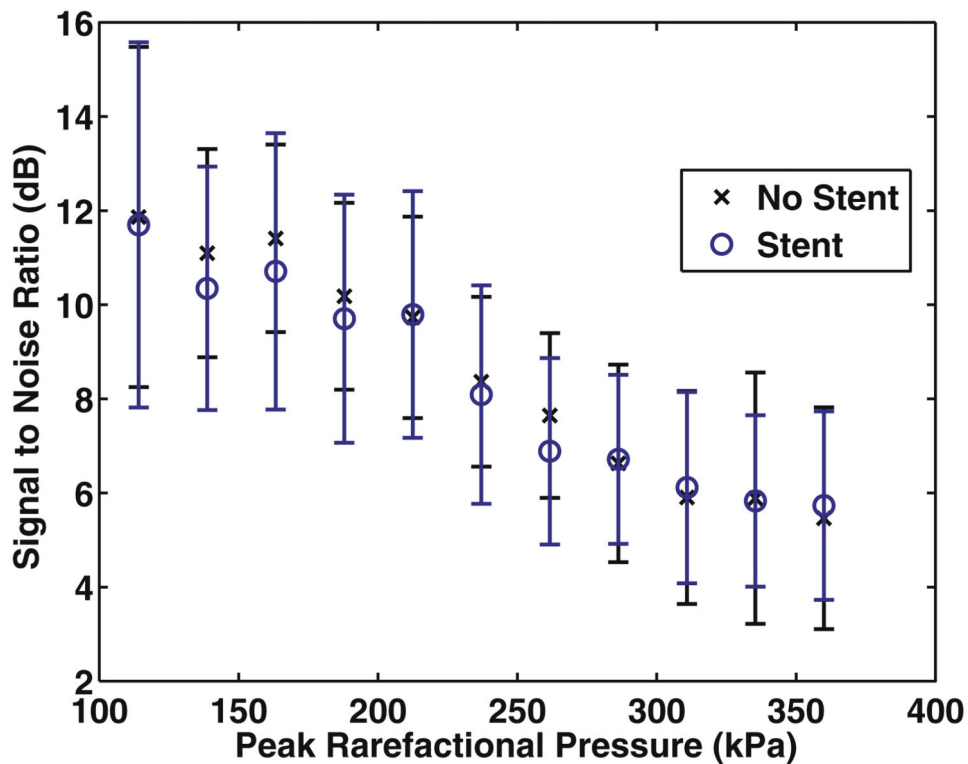


Fig. 4.

Signal-to-noise ratios for ultraharmonic emissions within the passive cavitation images. A region of interest was defined within the stent or at an equivalent location for data acquired without a stent. The mean ultraharmonic emission power and inharmonic emission power within this region of interest were calculated with and without the stent in the flow system. The ratio of ultraharmonic power to inharmonic power was defined as the signal-to-noise ratio. Power in the inharmonic bands was due to spectral leakage from the harmonics, broadband emissions from inertial cavitation or a combination.

OFP-ELIP = octafluoropropane echogenic liposomes.

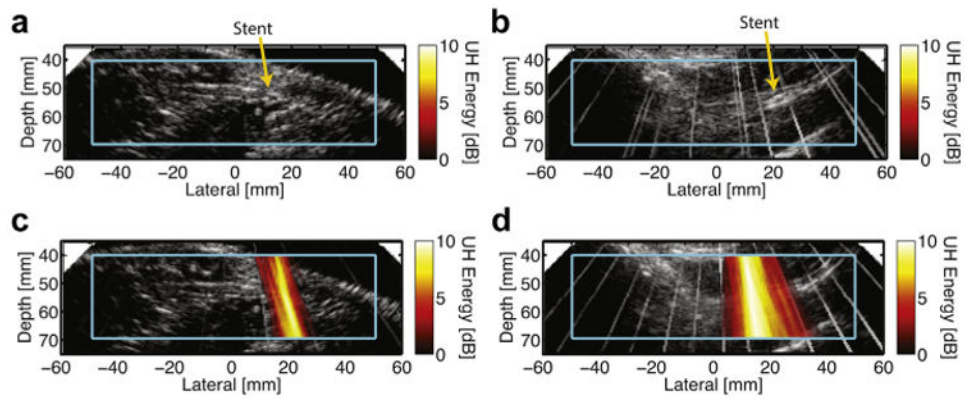


Fig. 5.

Exemplar duplex passive cavitation images with and without OFP-ELIP. The stent (*orange arrow*) was insonified with 500-kHz pulsed therapeutic ultrasound at a mechanical index of 0.24 (a, c) or 0.51 (b, d). The therapeutic ultrasound insonation created artifacts that appear as rays in the B-mode image. Insonations were performed with (c, d) and without (a, b) an OFP-ELIP injection. Stable cavitation activity, indicated by the ultraharmonic energy was detected only in the presence of the therapeutic ultrasound and OFP-ELIP. Higher insonation pressure amplitudes generally resulted in higher amplitude and more spatially distributed cavitation activity. OFP-ELIP = octafluoropropane echogenic liposomes, UH = ultraharmonic.

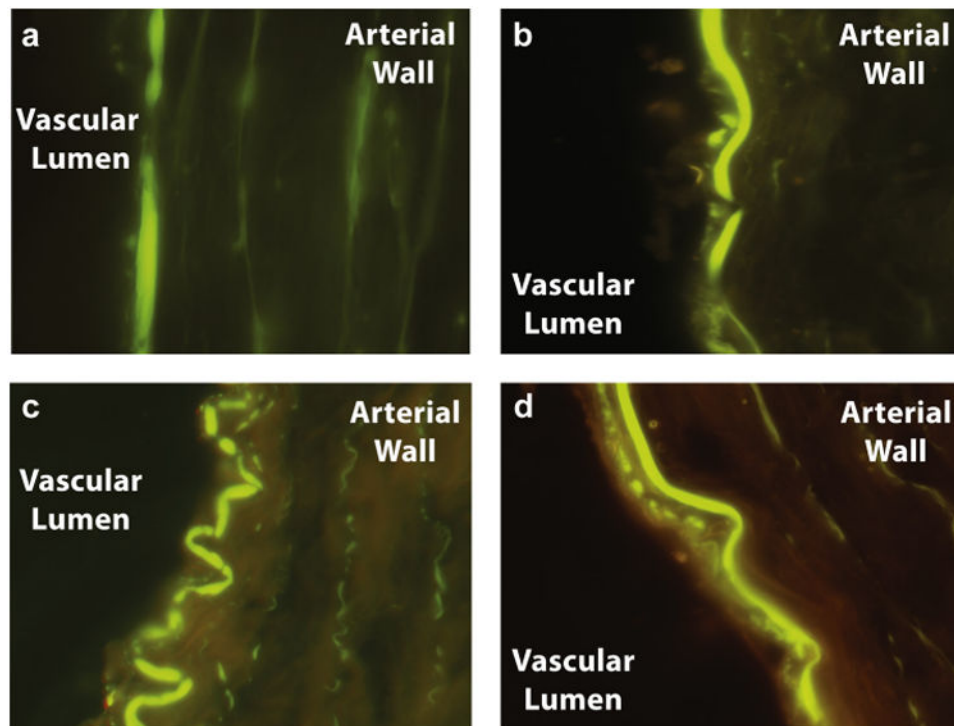


Fig. 6.

Delivery of anti-VCAM-1 rhodamine-labeled OFP-ELIP to the vascular wall. Composite fluorescence images were obtained by combining images taken with a fluorescein isothiocyanate filter detecting tissue autofluorescence and a red filter detecting rhodamine. (a) The femoral artery that was not exposed to 500-kHz ultrasound had no increase in red fluorescence in the media relative to the lumen. (b) The femoral artery that was exposed to 500-kHz therapeutic ultrasound and anti-VCAM-1 rhodamine-labeled OFP-ELIP, but from which no ultraharmonic emissions were detected, did not exhibit increased red fluorescence in the media relative to the lumen. (c, d) Femoral arteries that were exposed to therapeutic ultrasound and anti-VCAM-1 rhodamine-labeled OFP-ELIP and from which ultraharmonics were detected did exhibit an increase in red fluorescence in the media relative to the lumen. OFP-ELIP 5 octafluoropropane echogenic liposomes, VCAM-1 = anti-vascular cell adhesion protein 1.